Prediction of Cavitation Erosion: An Energy Approach

Data · January 2014

CITATIONS
29

READS
430

3 authors, including:

François Avellan
École Polytechnique Fédérale de Lausanne
421 PUBLICATIONS **6,790** CITATIONS
SEE PROFILE

Philippe Dupont
Zurich University of Applied Sciences ZHAW
57 PUBLICATIONS **685** CITATIONS
SEE PROFILE

Prediction of Cavitation Erosion: An Energy Approach

F. Pereira
Research Associate.

F. Avellan
Professor.

Ph. Dupont
Research Associate.

IMHEF-EPFL,
Institut de Machines Hydrauliques
et de Mécanique des Fluides,
Swiss Federal Institute of Technology,
Av. de Cour 33, 1007 Lausanne,
Switzerland

The objective is to define a prediction and transposition model for cavitation erosion. Experiments were conducted to determine the energy spectrum associated with a leading edge cavitation. Two fundamental parameters have been measured on a symmetrical hydrofoil for a wide range of flow conditions: the volume of every transient vapor cavity and its respective rate of production. The generation process of transient vapor cavities is ruled by a Strouhal-like law related to the cavity size. The analysis of the vapor volume data demonstrated that vapor vortices can be assimilated to spherical cavities. Results are valid for both the steady and unsteady cavitation behaviors, this latter being peculiar besides due to the existence of distinct volumes produced at specific shedding rates. The fluid energy spectrum is formulated and related to the flow parameters. Comparison with the material deformation energy spectrum shows a remarkable proportionality relationship defined upon the collapse efficiency coefficient. The erosive power term, formerly suggested as the ground component of the prediction model, is derived taking into account the damaging threshold energy of the material. An erosive efficiency coefficient is introduced on this basis that allows to quantify the erosive potential of a cavitation situation for a given material. A formula for localization of erosion is proposed that completes the prediction model. Finally, a procedure is described for geometrical scale and flow velocity transpositions.

Introduction

The present work has been initiated in the frame of the multidisciplinary and long-standing problem of the prediction of cavitation erosion in hydraulic machines.

The energy approach is based on the determination of the energy spectrum associated with a leading edge cavitation. The collapse of vapor cavities at the rear part of an attached cavity is known to be capable of damage on most types of materials. However, the experimental determination of this spectrum has not been attainable up to now and, as a consequence, no prediction model has received enough consensus to be widely applied.

Prior investigators have put forth great effort in (*i*) understanding the fluid mechanisms originating such extremely high stresses, and (*ii*) improving the performance of materials.

There is a global agreement about the fact that cavitation erosion results from the repeated collapse of vapor structures in the neighborhood of rigid boundaries. However, the basic mechanism has been much debated. The focus of prior work may be categorized as described below.

The first explanation, even though theoretical, has been proposed by Rayleigh (1917) whose model describes the time evolution of the radius of a vapor bubble in an infinite fluid medium at constant pressure. A local and very high pressure peak appears in the final collapse stage. Fujikawa and Akamatsu (1980) showed that this pressure peak was associated with a shock wave that they pointed out as the main damaging factor.

Kornfeld and Suvorov (1944), Vogel et al. (1989) demonstrated that vapor bubbles do not collapse spherically in the neighborhood of solid boundaries or when subjected to pressure gradients. They observed a liquid microjet threading the bubble and finally striking and damaging the boundary.

Although the damaging process is certainly a combination of these two mechanisms, recent works indicate that the shock wave is probably the predominant one: Avellan and Farhat (1989), Fortes-Patella and Reboud (1993).

The generation process of vapor cavities by a leading edge cavity has been often described (Knapp et al., 1970; Kubota et al., 1987; Farhat et al., 1993). In particular, steady and unsteady behaviors have been reported. The former situation is characterized by small scale vapor cavities shed with no obvious periodicity. Instead, the unsteady cavitation is recognizable by the periodic shedding of large scale vapor structures, ruled by a Strouhal law. Often called cloud cavitation, this behavior is generally considered as the most erosive situation.

Therefore, cloud cavitation has motivated and yet motivates a great amount of experimental and numerical research work: noise generation (Bark and Berlekom, 1978), erosion (Franc and Michel, 1988; Kato et al., 1996), cloud collapse (Soyama et al., 1992), bubble interaction and shock wave propagation (Mørch, 1981; Chahine and Duraiswami, 1992).

Along with the prediction problem, transposition laws are needed in what concerns testing of hydraulic machines, to transpose prediction outputs from laboratory tests on small scale model to full scale machine. Attempts have been made in the past in that direction: Thiruvengadam (1971), Kato (1975).

Notably, Bourdon et al. (1990) and Farhat et al. (1993) developed the notion of erosive power through the P_{er} term, introduced as a scaling factor for cavitation erosion in hydraulic machines. Promising results were obtained (Farhat, 1994), and stimulated and oriented the present study.

The only reasonable approach to the problem of predicting cavitation erosion consists in the conciliation of the two aspects of the phenomenon: fluid and material. Specifically, this should be done through the determination of the erosive potential of the cavitation situation under consideration. Unfortunately, it appears from our literature review that very few studies are related to the understanding of the energy transfer between the main flow and the material. Hammitt (1963) is a pioneer in this aspect as he hypothesized a model for cavitation erosion based on the knowledge of the energy spectrum $\mathbf{n}(E_c)$, where E_c is the potential energy of a vapor cavity.

In our study, we consider the problem of cavitation erosion following the so-called energy approach inspired by this investigator. This approach appears to be particularly suitable for the definition of an erosion prediction tool. Moreover, the erosive

Contributed by the Fluids Engineering Division for publication in the JOURNAL OF FLUIDS ENGINEERING. Manuscript received by the Fluids Engineering Division July 11, 1997; revised manuscript received April 30, 1998. Associate Technical Editor: J. Katz.

power term P_{er} is a privileged basis towards this definition. We intend to validate the energy approach by the measurement and analysis of two ground components of P_{er}: V_c and f_c. The third term, Δp, is accessible either from direct pressure measurements (see Farhat, 1994; Pereira, 1997), or from flow computation, and therefore is not considered in the frame of the current work.

Cavitation tests are performed in the IMHEF's high speed cavitation tunnel, on a symmetrical hydrofoil NACA 65012 (chord length is 100 mm). Steady and unsteady cavitation behaviors are studied.

In a first part, a new event counting technique combined with a wavelet analysis is presented as to determine the rate of production of transient vapor vortices by the leading edge cavity. Afterwards, a visualization technique, combining principles of stereometry and tomography, is introduced to determine the volume of vapor cavities through their tridimensional reconstruction.

Results are discussed in the second part. On the one hand, the generation process of transient vapor cavities is analyzed on a statistical basis from which an analytical formulation of the production rate is carried out. On the other hand, data from the volume reconstruction are analyzed with a view to the modeling of volumes while ensuring the cohesion with the production laws.

In a third and concluding part, we perform a global synthesis where we develop the formalism of the energy approach. The energy spectrum is analytically expressed as a function of the main flow parameters. The erosive power term P_{er} is derived while integrating the concept of damaging threshold energy introduced by Hammitt (1963). Then, prediction and transposition aspects are considered and formulated according to these fundamental definitions. Finally, elements for an experimental validation of the energy approach are presented, comparing the spectrum of the fluid energy and that of the material deformation energy.

Production Rate of Vapor Cavities

Principle and Instrumentation. A technique is brought into operation to carry out the production rate of transient vapor cavities (also referred to as vortices) in relation with their characteristic size λ. The setup is depicted in Fig. 1. A coherent light beam provided by a 5 W laser source is focused on a reflecting area of the hydrofoil. The beam is pointed onto the closure region of the main cavity and is oriented perpendicularly to the profile surface so that the incident and the reflected beams have the same path.

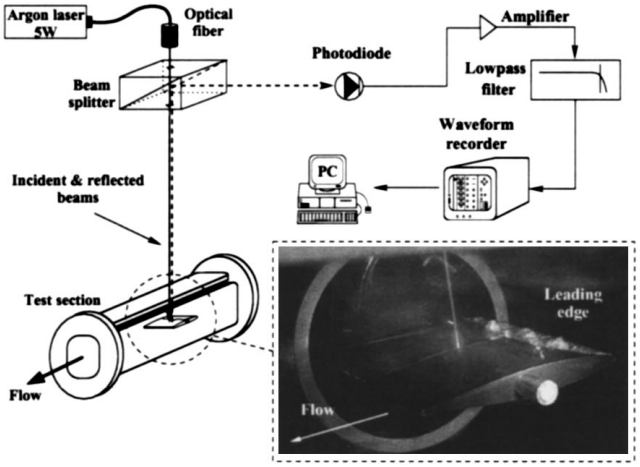

Fig. 1 Production rate of vapor vortices: experimental setup

By means of a splitter cube, the reflected beam is deflected 90° towards an ultrafast photodiode (rise time: 1 ns). The voltage signal output of this sensor is filtered and amplified to compensate losses due to the successive passages through the splitter cube. Therefore, the voltage signal is ideally maximum when total reflection is observed and attenuated when a vapor cavity passes through the beam.

Three hypotheses are considered: (*i*) Vapor cavities are opaque and diffusive objects; (*ii*) The characteristic size λ of a cavity corresponds to its longitudinal maximum extent; (*iii*) Vapor cavities are produced spanwise according to the same process (though with a phase shifting that currently is not measured).

Provided an adequate signal processing, the cavity characteristic size λ may be determined from the knowledge of the light extinction time and of the convection velocity C_c. The production rate of cavities in a given size range comes out from their counting over the measurement period.

The photodiode signal is filtered at 100 kHz and sampled at 200 kHz over multiple time periods of 2.6 s each.

Data Processing and Analysis. The wavelet analysis, and namely the continuous wavelet transform (CWT, see Farge, 1992), was found to be the most appropriate technique to deter-

Nomenclature

C_c = convection velocity, $m \cdot s^{-1}$
C_{ref} = upstream flow velocity, $m \cdot s^{-1}$
d_{eq} = equivalent diameter of vapor cavity, m
E_a = acoustical energy of vapor cavity, J
E_c = potential energy of vapor cavity, J
E_d = damaging energy of material, J
E_m = maximum potential energy of vapor cavity, J
E_s = minimal damaging energy of material, J
f_c^{λ} = shedding frequency of cavities with size λ, Hz
f_c = main shedding frequency, Hz
i = flow angle of incidence, °
l = length of main cavity, m
L = chord of hydrofoil, m
$\mathbf{n}$ = frequency histogram, s^{-1}
$\hat{\mathbf{n}}$ = statistical density, $\hat{\mathbf{n}}(\lambda)$ $m^{-1} \cdot s^{-1}$, $\hat{\mathbf{n}}(E_c)$, $J^{-1} \cdot s^{-1}$
$\hat{\mathbf{N}}$ = statistical distribution, s^{-1}
$\tilde{\mathbf{N}}$ = normalized distribution, $\tilde{\mathbf{N}} = \hat{\mathbf{N}}/C_{ref}$, m^{-1}
p_{ref} = upstream pressure, Pa
p_v = vapor pressure, Pa
P_{er} = erosive power, W
R_m = bubble initial radius, m
t_r = Rayleigh time, s
V_c = volume of transient vapor cavity, m^3
x_c = abscissa of collapse location, m
δ_c = displacement of convected vapor cavity, m
Δp = pressure difference in the main cavity closure region, Pa
$\lambda_{x,y,z}$ = main dimensions of a vapor cavity, m
α, β = statistical class parameters
C_p = pressure coefficient, $C_p = (p - p_{ref})/(\frac{1}{2}\rho C_{ref}^2)$
$C_{p_{max}}$ = C_p in the main cavity closure region
η_{co} = collapse efficiency, $\eta_{co} = \hat{\mathbf{n}}(E_d)/\hat{\mathbf{n}}(E_c)$
η_{er} = erosive efficiency, $\eta_{er} = 1 - (E_s/E_m)^{2/3}$
λ_{er} = erosive power coefficient
σ = cavitation coefficient, $\sigma = (p_{ref} - p_v)/(\frac{1}{2}\rho C_{ref}^2)$
S_c = production rate constant, $S_c \simeq 86.87\ 10^{-3}$
S, S_c^{α} = Strouhal numbers, $S = (f_c l)/C_{ref}$ $S_c^{\alpha} = S_c\alpha/(1 + \alpha)$
RMS = root mean square error on least squares fitted data

mine the production rate of vapor cavities accordingly to their individual characteristic length. In contrast with the Fourier transform, this analysis is particularly suitable for random and transient signals, being yet applicable to the detection of periodicities (as expected in the case of cavitation unsteadiness).

The original wavelet analysis is a convolution of the original signal $f(t)$ with a wavelet function $\psi(t)$, the so-called mother wavelet. The CWT is a generalization procedure of this convolution operation that uses a family of wavelet functions $\psi_{\kappa,\tau}(t)$ continuously translated (parameter τ) and dilated (parameter κ). Thus, it performs a transformation between the physical time space t and a time-scale space (t, ϕ). The complex-valued Morlet wavelet is currently used. The following analysis is obtained:

$$\tilde{f}(\kappa, \tau) = \langle \psi_{\kappa,\tau} | f \rangle = \kappa^{-1/2} \int_{\mathbf{R}} \psi^* \left(\frac{t-\tau}{\kappa} \right) f(t) dt \quad (1)$$

ψ^* is the complex conjugate of ψ and $\tilde{f}$ is the CWT of $f(t)$.

Another important aspect of this transform is the conservation of energy locally (and therefore globally), see Lewalle (1994). The CWT is usually represented by the energy density map: local energy spectral density plotted versus time t and scale ϕ.

Because the water fluid contains microbubbles of undissolved air, the light signal may get noisy. Therefore, the voltage signal from the photodiode is processed in a two steps procedure before the wavelet analysis: (*i*) Subtraction of the off-cavitation voltage; (*ii*) Envelope in a frequency range of 0–100 kHz (using the Hilbert transform).

Finally, the cavity characteristic size λ is related to the ϕ scale through the following relation: $\lambda = K(C_c/\phi)$, where K is a normalization coefficient and C_c is the convection velocity of the vapor structure in the closure region of the main cavity. Considering the experimental results carried out by Kiya and Sasaki (1983) ($0.5\ C_{\text{ref}}$) and Farhat (1994) ($0.65\ C_{\text{ref}}$), we take $C_c = 0.6\ C_{\text{ref}}$. We emphasize the fact that this convection velocity is only valid at the measurement location.

It is noteworthy that the primary concepts in the wavelet analysis are those of time and scale, whereas frequency is clearly a secondary quantity obtained from the repetition of individual events. Let an event be the occurrence of a cavity of size λ at an instant t. An algorithm (see Pereira, 1997) is developed that locates every maximum appearing in the energy map, thus giving an equal importance to low and high energy events. The resulting image is called the structure map from which the event histogram $\mathbf{n}$ is carried out. Dividing this quantity by the measurement period gives the frequency f_c^{λ} associated to the size class λ. We refer $\hat{\mathbf{n}}$ as the statistical density and $\hat{\mathbf{N}}$ as the statistical distribution associated to class λ.

Eight data segments of 32 *k*-samples each ($\approx$164 ms) are processed. The ϕ scale is divided into 9 octaves with 16 voices each (therefore, we have 144 λ classes). Lengths λ in the range 0.5 to 100 mm are considered.

Volume of Vapor Cavities

Principle and Instrumentation. The quantification of two phase phenomena in terms of volume or shape data is technically complex. Most current visualization techniques are only applicable when geometrical characteristics are considered steady in time, such as in the case of the leading edge cavity: laser sheet (Farhat et al., 1993), high speed photography (Lehman, 1966), holography (Maeda et al., 1991), tomography (Levinthal and Ware, 1972), etc. However, the vapor structures produced by a leading edge cavity are characterized by a very short lifetime, an extremely changing shape and are conveyed by the flow at high speeds (up to 50 $\text{m}\cdot\text{s}^{-1}$ in the test section of the IMHEF-LMH's cavitation tunnel).

To quantify the geometrical characteristics of these transient vapor vortices, we developed a technique combining principles of tomography and stereometry, see Pereira (1997). The basic and intuitive principle is that the volume of an object in space (moving or not) can be estimated out from simultaneous contours taken from a minimum of two noncollinear lines of sight. Contours define, in the 3-D space, cylinders (or cones) that encompass the object being observed. They intersect each other and form a common volume that overestimates the real volume. Accuracy can be increased with a higher number of contours.

Four black and white frame transfer CCD cameras are arranged around the test section according to Fig. 2.

In monoshot mode, the CCD integration period (20 ms) starts on a TTL signal input. Afterwards, the image information is transferred onto a storage section where it remains until a TTL readout signal is received. Information is finally converted to standard video signal and output to a 8-bits frame grabber. Archiving is done on S-VHS video tape. Special electronic hardware was developed for the conditioning of the video signal as well as for the camera control from a remote computer (addressing, multiplexing, triggering, gain control and synchronization between video devices). A compact mechanical mounting has been designed for each camera, allowing precise positioning (1 rotation and translation on 3 axes). Lighting is undertaken by two flash point sources placed around the test section. Flashes are triggered randomly during camera integration period to avoid any coupling with the phenomenon being observed. The trigger pulse is transmitted through an optical fiber in order to protect electronics hardware from electromagnetic disturbances.

Images are acquired simultaneously on all four cameras and readout sequentially according to the above sequence. The cycle takes 140 ms from acquisition to storage and is repeated 512 times at the corresponding frequency ($\approx$7 Hz).

Data Processing and Analysis. Volume extraction goes through 4 steps: (*i*) image enhancement: normalization to full pixel range (256 grey levels) and thresholding; (*ii*) contour extraction by gradient operator; (*iii*) contour closing; (*iv*) volume intersection. The intersection operation is the core of the volume reconstruction (see Pereira, 1997). This procedure is applied to all possible pairs of object contours. An orthogonal parallelepiped is drawn out that encompasses the intersection points and is divided into voxels (discrete volume elements). Each voxel is defined by a center, an elementary volume and a norm. This norm is equal to unity if the projection of the associated center on at least one image plane is inside the corresponding contour, 0 if on the contour and -1 on the outside.

Total volume of object under consideration is the summation of all elementary volumes from voxels whose norm is zero or unity. Figure 3 shows the graphical display of the final reconstructed volume of an upside down U-shaped vapor vortex. Upper four photographs are the simultaneous images from the CCD cameras and bottom figures show the reconstructed cavity. It clearly demonstrates the ability of the technique to closely catch complex 3-D structures.

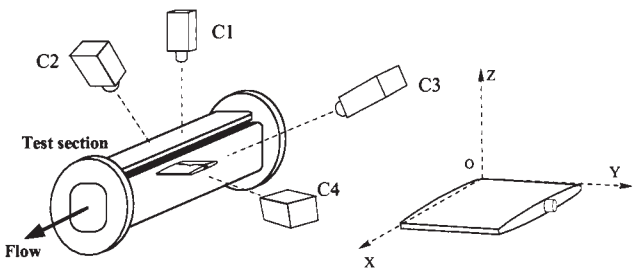

Fig. 2 Cameras arrangement around test section and world coordinates system

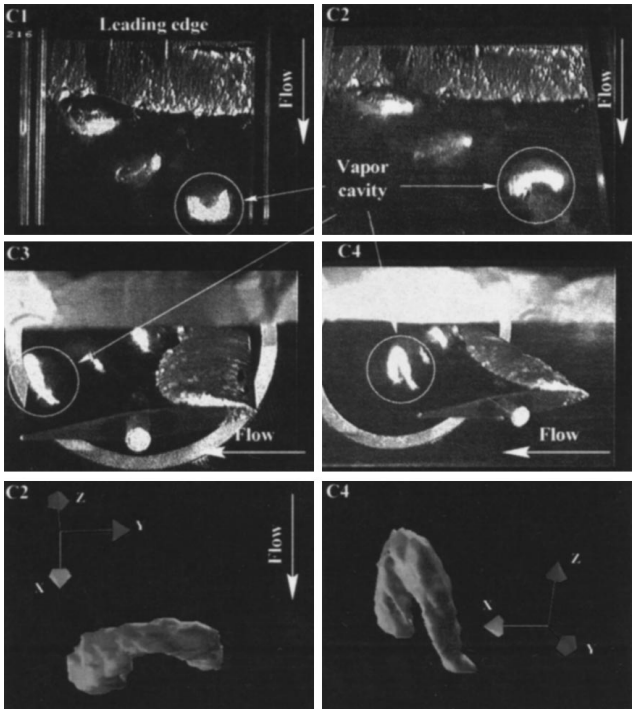

Fig. 3 Reconstruction of a vapor volume

Calibration. Calibration of a stereoscopic system is the process by which we determine the geometrical and optical characteristics of a camera (intrinsic parameters) and/or the 3-D position and orientation in the world space of the image sensor (extrinsic parameters). Eleven parameters (6 extrinsic and 5 intrinsic) are determined by our algorithm (see Pereira, 1997). World space coordinates may be derived from multiple image data and vice versa. Minimum measurable volume is 0.44 mm^3.

Flow Conditions

We explored 2 flow angles of incidence (4 and 6 deg), 3 main cavity lengths (l/L = 20, 30, 40 percent) and 5 upstream flow velocities (C_{ref} = 15, 20, 25, 30, 32 $m \cdot s^{-1}$). The cavitation coefficient σ is adjusted to obtain the correct main cavity length, which is checked under continuous lighting by means of a graduated video monitor. As soon as flow parameters are considered steady in time, 128 measurements are performed and averaged over a period of 30 s before the image acquisition loop.

Results and Discussion

Production Rate of Vapor Cavities. Figure 4 represents $\tilde{\mathbf{N}}$, which is the event statistical distribution $\hat{\mathbf{N}}$ (number of events $\geq\lambda$ per unit of time) divided by the respective mean flow velocity C_{ref}. $\tilde{\mathbf{N}}$ is plotted versus structure size λ. Only sizes below 50 mm are reported since structures with characteristic size greater than the main cavity mean length can reasonably be put aside.

It follows from these graphs (see Pereira, 1997) that the distributions $\hat{\mathbf{N}}$ are ruled by the relation $\hat{\mathbf{N}}(\lambda) = kC_{ref}/\lambda$, where k is a constant. The analytical formulation of the event density $\hat{\mathbf{n}}(\lambda)$ can be derived from this analysis:

$$\hat{\mathbf{n}}(\lambda) = k\,\frac{C_{ref}}{\lambda^2}, \quad k \simeq 86.87\ 10^{-3} \pm 12\ 10^{-5} \qquad (2)$$

The number of events per unit of time $\mathbf{n}(\lambda)$ is given by the following relation:

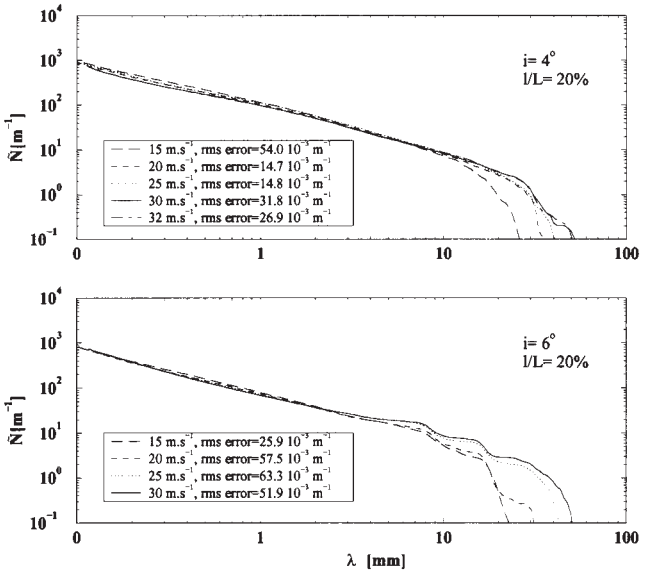

Fig. 4 Normalized distributions $\tilde{N} = \hat{N}/C_{ref}$ versus λ. i = 4°, 6°, l/L = 20%

$$\mathbf{n}(\lambda) = \int_{\lambda}^{\lambda+\Delta\lambda} \hat{\mathbf{n}}(\zeta)\,d\zeta \qquad (3)$$

$\mathbf{n}(\lambda)$ is the so-called production rate (or shedding frequency) of vapor cavities in the interval $[\lambda, \lambda + \Delta\lambda]$, and will be now referred to as f_c^{λ}. We show that f_c^{λ}, C_{ref} and λ are linked by the relation

$$\frac{\lambda f_c^{\lambda}}{C_{ref}} = S_c\,\frac{\alpha}{1+\alpha} = S_c^{\alpha}, \quad S_c \simeq 86.87\ 10^{-3} \pm 12\ 10^{-5} \qquad (4)$$

where α is a parameter defining the density class width: $\alpha \in \mathbf{R}^+ | \Delta\lambda = \alpha\lambda$. S_c is the production rate constant and is equal to k of relation (2). S_c^{α} tends to S_c as α grows to infinity.

Figure 5 represents the values of S_c^{α} when formula (4) is applied to the experimental histograms $\mathbf{n}$. In the case of our analysis, we have $\alpha \simeq 43.3\ 10^{-3}$. S_c^{α} is found constant and close to $3.8\ 10^{-3}$ over the whole λ scale. This result fully validates the above reasoning and shows that the generation

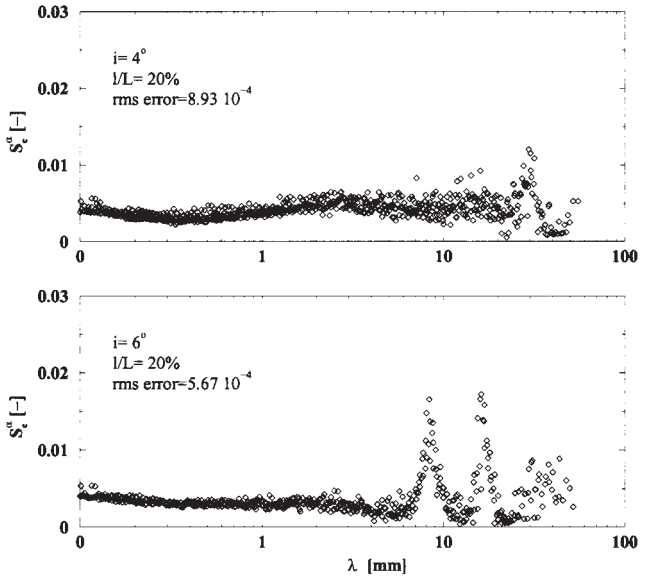

Fig. 5 Strouhal number S_c^{α} versus λ. i = 4°, 6°, l/L = 20%

process of the transient vapor cavities is truly ruled by the Strouhal-like law of Eq. (4), provided α is chosen (even arbitrarily).

The unsteady case ($i = 6$ deg) is characterized by two particular λ values that we call λ_1 and λ_2. We show that these singular lengths are essentially defined by the main cavity mean length according to the following relations: $\lambda_1 \simeq 0.44l$ and $\lambda_2 \simeq 0.85l$. Considering the uncertainties related to the convection velocity determination, we point out that these values are comparable with the $\frac{1}{3}$ and $\frac{2}{3}$ values that are commonly found in the literature as far as the generation process of vapor cavities in the unsteady situation is discussed. As a matter of fact, these results are coherent with the 3-parts cyclic generation sketches proposed by Le et al. (1993) and Kubota et al. (1987).

Finally, let f_c be the sum of frequencies f_c^{λ} of events whose dimension λ is in the close vicinity of λ_1 and λ_2. f_c is called the macroscopic or main shedding frequency. Figure 6 represents this frequency versus the reduced frequency C_{ref}/l.

This graph clearly shows that the production rate of vapor cavities inside these two λ classes is controlled by the well-known Strouhal law based on the main cavity length and on the upstream flow velocity:

$$S = \frac{f_c l}{C_{\text{ref}}} \quad \text{with} \quad S \approx 0.3 \tag{5}$$

This result is perfectly coherent with those found in literature related to unsteady cavitation behavior: Simoneau et al. (1989), Farhat et al. (1993), Farhat (1994), Kubota et al. (1987), Le et al. (1993).

Volume of Vapor Cavities. We showed (Pereira, 1997) that the most relevant information, with respect to the volume of vapor cavities, were the dimensions λ_x, λ_y, and λ_z, respectively the chordwise, the spanwise, and the vertical extents.

Figure 7 shows that there exist linear relationships between λ_x, λ_y, and λ_z. We have reported couples (λ_x, λ_y) and (λ_y, λ_z) (values are divided by l), accompanied by the corresponding linear regression. λ_x and λ_y are identical with a slope coefficient close to unity, for both the steady and unsteady cases ($\lambda_y \approx 0.851\lambda_x$ and $\lambda_y \approx 1.035\,\lambda_x$, respectively). Graphs related to (λ_y, λ_z) show that the cavity height is about 60% higher than λ_y (slopes are 1.629 and 1.582, respectively for $i = 4$ deg and $i = 6$ deg). Besides, the unsteady case ($i = 6$ deg) is characterized by two secondary trends indicating that there exist two

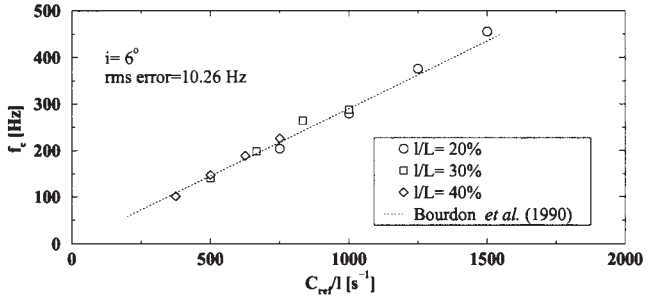

Fig. 6 Shedding frequency f_c versus reduced frequency C_{ref}/l. $i = 6°$, $l/L = 20, 30, 40\%$

additional volume families that confirm the following relations: $\lambda_z \approx 0.197\lambda_y$ and $\lambda_z \approx 0.562\lambda_y$. As established by Pereira (1997), we also have $\lambda_y \approx 1.61\lambda_x$ and $\lambda_y \approx 2.17\lambda_x$. It is also noticeable that the longitudinal and transversal dimensions (λ_x and λ_y) rarely exceed half of the main cavity length l in the steady situation. Instead, for $i = 6$ deg, λ_x and λ_y may equal it, while appearing the aforementioned two specific types of volumes. These remarks are in full agreement with the visual observations.

Because experimental volume data were not available up to now, vapor structures produced by the leading edge cavity were usually considered to be spherical volumes (Kato, 1975; Selim, 1985; Baiter, 1982). Our immediate purpose is to check the validity of this hypothesis. Let $d_{\text{eq}} = \sqrt[3]{(6/\pi)V_c}$ be the equivalent diameter. Figure 8 represents dimensions $\lambda_{x,y,z}$ versus d_{eq}. In the steady case (4 deg), these dimensions vary linearly with the equivalent diameter and slopes are similar to that found above between λ_x, λ_y and λ_z. For $i = 6$ deg (unsteady behavior), multiple trends appear on graph (d_{eq}, λ_z). The main trend indicates that λ_z is about 60 percent greater than d_{eq}. Secondary trends are related to the specific volumes that characterize the unsteady case. Slopes are close to that found between λ_z and λ_y (Fig. 7).

As a consequence, d_{eq} is representative of dimensions $\lambda_{x,y,z}$ of vapor volumes. Table 1 reports the relationships between $\lambda_{x,y,z}$ and d_{eq} as well as the constants that provide, from the single knowledge of the main cavity mean length, the $\lambda_{x,y,z}$ dimensions of the macroscopic structures produced in the un-

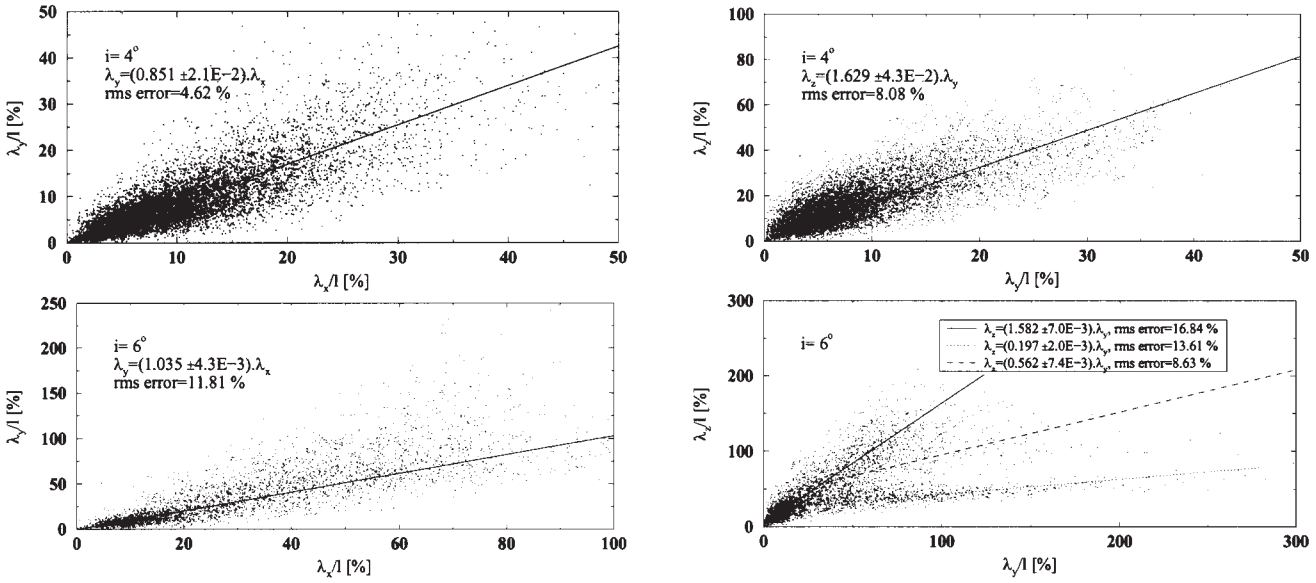

Fig. 7 Relationships between dimensions $\lambda_{x,y,z}$. $i = 4°, 6°$, $C_{\text{ref}} = 15, 20, 25, 30, 32\ \text{m}\cdot\text{s}^{-1}$, $l/L = 20, 30, 40\%$

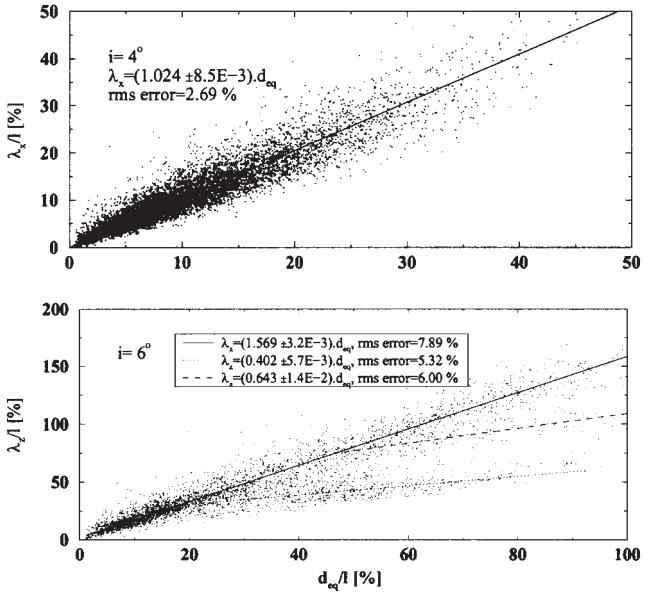

Fig. 8 $\lambda_{x,y,z}$ **versus the equivalent diameter** d_{eq}. $i = 4°, 6°$, $C_{ref} = 15, 20, 25, 30, 32\ m \cdot s^{-1}$, $l/L = 20, 30, 40\%$

steady cavitation behavior. These characteristic dimensions are coherent with visual observations and high speed visualizations: Farhat (1994), Brennen (1994), Kubota et al. (1987).

Energy Approach: Formalism and Validation

The energy spectrum suggested by Hammitt (1963) describes the energy transfer between the fluid and the material. This concept is illustrated on Fig. 9, for different cavitation extents: the coordinate axis represents the frequency histogram $\mathbf{n}(E_c)$ of cavities with potential energy inside the interval $[E_c, E_c + \Delta E_c]$.

Hammitt emphasizes the fact that he takes into account only the cavities that effectively produce damage, suggesting that an energy E_s exists beyond which damage takes place. This threshold, reported on Fig. 9, depends on the mechanical properties of the material under consideration. Thus, the damaging energy is proportional to the surface under the curve corresponding to the cavitation extent, with $E_c \geq E_s$.

Energy Density. The energy density $\hat{\mathbf{n}}(E_c)$ is related to the event density $\hat{\mathbf{n}}(\lambda)$ by

$$\hat{\mathbf{n}}(E_c)dE_c = \hat{\mathbf{n}}(\lambda)d\lambda \tag{6}$$

where λ is the longitudinal maximum extent of cavities, as hypothesized formerly. Furthermore, Table 1 shows that the dimensions $\lambda_{x,y,z}$, and specifically the longitudinal one, are proportional to d_{eq}, with $d_{eq} \propto \sqrt[3]{V_c}$. Thus, the potential energy E_c of a cavity may be expressed by

Table 1 Dimensional characteristics of vapor volumes

Steady		Unsteady		
Eq. (4)	Eq. (5)	Eq. (4)		Eq. (5)
$\lambda_x \approx d_{eq}$	—	$\lambda_x \approx d_{eq}$		$\lambda_x = 0.44\ l$
$\lambda_y \approx d_{eq}$	—	$\lambda_y \approx d_{eq}$	1	$\lambda_y = 0.71\ l$
$\lambda_z \approx 1.6\ d_{eq}$	—	$\lambda_z \approx 1.6\ d_{eq}$		$\lambda_z = 0.14\ l$
				$\lambda_x = 0.85\ l$
			2	$\lambda_y = 1.84\ l$
				$\lambda_z = 1.04\ l$

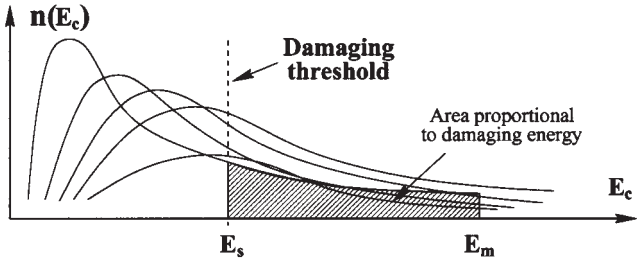

Fig. 9 Energy spectra according to Hammitt (1963)

$$E_c = \Delta p V_c \propto \Delta p \lambda^3, \quad \Delta p = \tfrac{1}{2}\rho(\sigma + C_{p_{\max}})C_{\text{ref}}^2 \tag{7}$$

According to (7), we have $\lambda \propto E_c^{1/3}\Delta p^{-1/3}$. Thus, Eq. (6) becomes, using (2):

$$\hat{\mathbf{n}}(E_c) \propto C_{\text{ref}}\Delta p^{1/3}E_c^{-4/3} \tag{8}$$

Let $E_m = \Delta p \cdot l^3$ be the reference energy. E_m is normally associated with the maximum volume generated by the main cavity. However, we do not know the relationship between this volume and the current flow conditions, so we assume that this volume is proportional to l^3. This hypothesis is true in the unsteady situation, as suggested by Table 1.

The energy density $\hat{\mathbf{n}}(E_c)$ is finally given by

$$\hat{\mathbf{n}}(E_c) = K_0 S_c \frac{C_{\text{ref}}}{l} E_m^{1/3}E_c^{-4/3}, \quad K_0 = \sqrt[3]{\frac{\pi}{162}} \tag{9}$$

Energy Spectrum. The number per time unit of vapor cavities whose energy E_c is inside the interval $[E_c, E_c + \Delta E_c]$ is given by the relation:

$$\mathbf{n}(E_c) = \int_{E_c}^{E_c+\Delta E_c} \hat{\mathbf{n}}(\epsilon)d\epsilon \tag{10}$$

We introduce the parameter β that acts on E_c as α does on λ: $\beta \in \mathbf{R}^+ | \Delta E_c = \beta E_c$. Moreover, according to (6), we have the following relation:

$$\mathbf{n}(E_c) = \mathbf{n}(\lambda) = \int_{\lambda}^{\lambda+\Delta\lambda} \hat{\mathbf{n}}(\zeta)d\zeta = S_c \frac{C_{\text{ref}}}{\lambda} \frac{\alpha}{\alpha + 1} \tag{11}$$

Comparing coefficients from relations (10) and (11), we obtain the formulation of $\mathbf{n}(E_c)$:

$$\mathbf{n}(E_c) = K_1 S_c \frac{C_{\text{ref}}}{l} \left(\frac{E_m}{E_c}\right)^{1/3} [1 - (1 + \beta)^{-1/3}] \tag{12}$$

with

$$\beta = (1 + \alpha)^3 - 1 \quad \text{and} \quad K_1 = \sqrt[3]{\frac{\pi}{6}} \tag{13}$$

Spectrum $\mathbf{n}(E_c)$ is fully determined by the flow parameters. It differs from existing models based on theoretical probability laws selected to fit the closest possible the spectrum suggested by Hammitt (1963): Kato (1975), Selim (1985).

Collapse Efficiency. We assume that a vapor cavity induces damage if the energy resulting from the collapse is greater than the material threshold E_s. The damaging energy E_d issued from the cascade from flow to material is only a part of the initial fluid energy E_c. Knapp et al. (1970) estimated experimentally, being to our knowledge the only literature reference with regard to this aspect, that only 1 cavity in 30000 produces damage. Inspired on previous works (Ross, 1977; Baiter, 1982), we reintroduce the notion of collapse efficiency through the term η_{co}, which is a function of numerous parameters (energy

dissipation during collapse, distance of collapse to the wall, physical properties of fluid and material, roughness, pressure fluctuations, . . .). η_{co} is defined by the ratio between the spectrum of energy E_d absorbed by the material and that of energy E_c provided by the vapor cavities (with $E_c \geq E_s$):

$$\eta_{co} = \frac{\hat{\mathbf{n}}(E_d)}{\hat{\mathbf{n}}(E_c)} = \frac{\mathbf{n}(E_d)}{\mathbf{n}(E_c)} \tag{14}$$

Thus, η_{co} is only related to that part of collapses having energy larger than the threshold energy. It differs in that from the ''energy efficiency'' introduced by Reboud and Fortes-Patella (1996) as the ratio E_d/E_c, this being a measure of the effective energy transfer from flow to material. η_{co} is rather a macroscopic efficiency that integrates both the generation process and this energy cascade. We hypothesize that the collapse efficiency η_{co} is constant over the complete energy scale above E_s.

Erosive Power. The erosive power P_{er} (using the same terminology as Farhat et al., 1993) is the integral per time unit of energies contributing to the damage process (i.e., $E_c \geq E_s$):

$$P_{er} = \int_{E_s}^{E_m} \hat{\mathbf{n}}(\epsilon)\epsilon d\epsilon = K_2 S_c \frac{C_{\text{ref}}}{l} E_m \Phi_{\text{er}}, \quad K_2 = \sqrt[3]{\frac{\pi}{48}} \tag{15}$$

where E_m is the upper bound of energies. Term Φ_{er} is given by the relations:

$$\Phi_{er} = 1 - F^{2/3}, \quad F = \frac{E_s}{E_m} \tag{16}$$

Erosive Efficiency. We introduce the erosive efficiency η_{er} as the ratio between the erosive power and the total power of vapor cavities. η_{er} is a continuously decreasing function of the energy threshold E_s:

$$\eta_{er} = \frac{P_{er}}{\int_0^{E_m} \hat{\mathbf{n}}(\epsilon)\epsilon d\epsilon} = \Phi_{er} \tag{17}$$

The denominator represents the total energy per time unit and is proportional to the energy flux $(C_{\text{ref}}E_m)/l$.

Transposition. We consider two flows geometrically similar and with the same cavitation development (thus similar with regard to the cavitation coefficient σ). Fluid is unchanged.

The problem of transposition consists in studying the influence of a change of the flow velocity and/or of the geometrical scale. Let π_1 and π_2 be the transposition parameters: $\pi_1 = C'_{\text{ref}}/C_{\text{ref}}$ and $\pi_2 = l'/l$. C'_{ref} and l' are, respectively, the mean velocity and the main cavity length of the new flow. The cavity length is taken as the reference geometrical length due to the σ similarity.

Using Eqs. (15) and (16), the transposed erosive power P'_{er} is given by:

$$P'_{er} = \lambda_{er} P_{er}, \quad \lambda_{er} = \pi_1^3 \pi_2^2 \frac{1 - \Gamma F^{2/3}}{\eta_{er}}, \quad \Gamma = \pi_1^{-4/3} \pi_2^{-2} \tag{18}$$

λ_{er} is the erosive power coefficient: it allows the transposition of the erosive power P_{er}, both in velocity and in geometrical scale. It also includes the damaging energy threshold E_s as well as the macroscopic flow parameters of the original flow (through the erosive efficiency η_{er}).

Location of Collapse. According to the theoretical model developed by Rayleigh (1917), the time between the instant of application of pressure and the instant of zero radius is given by the Rayleigh time $t_r \cong 0.915\ R_m\sqrt{\rho/\Delta p}$, where R_m is the initial and maximum radius of the bubble. Four hypotheses are given: (*i*) According to Table 1, $\lambda = \lambda_x \simeq d_{\text{eq}}$; consequently, we can state that $R_m \approx \lambda/2$; (*ii*) Cavity is convected with the flow velocity $C_c = kC_{\text{ref}}$, $k \approx 0.6$; (*iii*) Δp is constant during t_r; (*iv*) Volume of cavity is maximum at abscissa l.

The displacement of a cavity is $\delta_c = t_r C_c$. Thus, using Eq. (7), the chordwise location of the collapse is given by

$$x_c = l\left[1 + K_3\left(\frac{E_c}{E_m}\right)^{1/3}(\sigma + C_{p_{\max}})^{-1/2}\right]$$

$$K_3 = \frac{0.915k}{\sqrt{2}}\sqrt[3]{\frac{6}{\pi}} \tag{19}$$

The collapse location is independent of the mean flow velocity, for a given flow incidence i and a given cavitation coefficient σ. This result is coherent with the works performed by Simoneau et al. (1989) and N'Guyen et al. (1987). For a given set of flow conditions, δ_c is proportional to λ. As a consequence, the collapse or pit density (number of collapses/pits per time unit and per length unit) may be expressed by: $\hat{\mathbf{n}}(\delta_c)d\delta_c = \hat{\mathbf{n}}(E_c)dE_c$. Equation (19) also points out that the beginning of the damaged area is fully determined when E_c equals E_s.

Experimental Validation: Elements. Pitting data is available from former erosion tests done independently of the present work, although on the same hydrofoil and for a subset of the flow conditions considered here. Cavitation tests were performed on Copper samples. Surface measurement was done using a laser profilometer and processed by a software developed by Fortes-Patella (1994) and co-workers. In addition to the geometrical characteristics of pits, the software provides the acoustical energy E_a associated to each pit and calculated according to the numerical simulation developed by this author.

Recent works (see Reboud and Fortes-Patella, 1996) indicate that the material deformation energy E_d is proportional to E_a, yet for a given material as long as this is strongly dependent upon the elastic properties of the material. As a consequence, we will use the terminology E_d instead of E_a to make clear distinction between flow and material. This is consistent since E_a is derived from material deformation data by the numerical simulation.

Figure 10 represents the energy spectra $\mathbf{n}(E_c)$ (fluid), calculated according to relation (12), and $\mathbf{n}(E_d)$ (material). Both are expressed per unit of surface. A remarkable proportionality relationship is noticed. The experimental spectra are fitted by power laws using a least squares method and are found to have exponents that closely match the theoretical exponent $-\frac{1}{3}$ of Eq. (12): -0.341 for $l/L = 20$ percent and -0.364 for $l/L = 40$ percent. One can estimate the collapse efficiency using Eq. (14). Figure 11 represents the value of η_{co} and shows that it remains fairly constant over the whole range of energies, thus confirming the hypothesis we made above.

Mean ratios between number of pits and number of cavities are found to be very low, ranging from 10^{-5} to 10^{-4}, as reported in Table 2. As a matter of fact, E_d can be much smaller than E_c or E_a, as reported by Reboud and Fortes-Patella (1996).

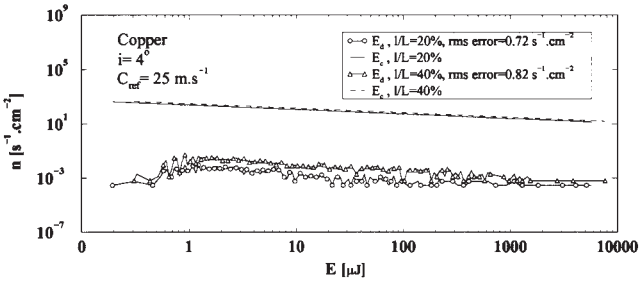

Fig. 10 Comparison of energy spectra between flow and material

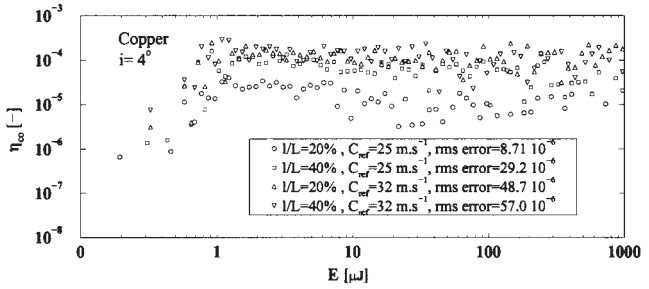

Fig. 11 Collapse efficiency $\eta_{co} = \hat{n}(E_d)/\hat{n}(E_c)$

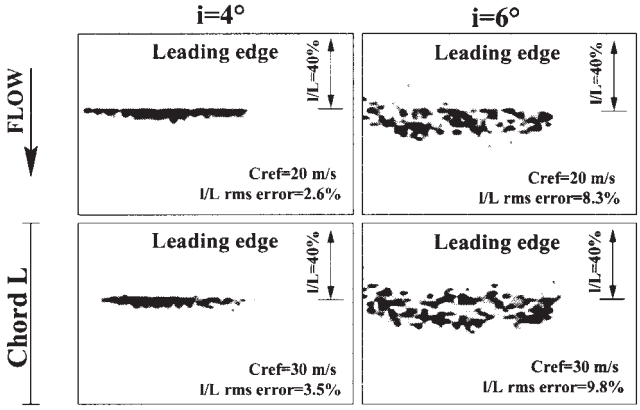

Fig. 12 Collapse locations of vapor cavities, top view: i = 4 deg, 6 deg, C_{ref} = 20, 30 m·s^{-1}, l/L = 40 percent

Moreover, the statistical density of vapor cavities decreases rapidly with their energy (see Eq. (9)). Yet, factors not fully understood, such as the distance of collapse to the wall, may be the main cause of such low values. Though, these values are quite coherent with those estimated experimentally by Knapp et al. (1970).

η_{co} is highly dependent upon the flow conditions. Curves relative to 25 m·s^{-1} and 32 m·s^{-1} point out that mean η_{co} increases with C_{ref}. These results are consistent with increased erosion observed by Simoneau et al. (1989). Influence of cavity length at constant velocity is not clearly established. Although flow parameters may act directly on η_{co}, they certainly have an indirect influence through complex phenomena: cloud structure, shock wave propagation, . . . These influences are beyond the objectives of the current study.

Relation (19) is used to determine the collapse area. Two main comments are suggested by the resulting collapse images of Fig. 12, confirmed by direct observation of eroded areas: (*i*) As stated earlier, the location of collapse is independent of C_{ref}; however, the distribution of collapses around the mean position changes: collapses move downstream when C_{ref} increases; this effect is mainly attributed to inertial forces and agrees with observed elongation of the main cavity with increasing C_{ref} (Dupont, 1991); (*ii*) For the unsteady case (6 deg), the collapse area enlarges around the mean position of the closure region; indeed, the energy spectrum widens and moves to higher energies, in particular because of the appearance of the characteristic volumes (see Table 1).

Conclusion

The production rate f_c^{λ} of transient vapor cavities generated by a leading edge cavity is ruled by a Strouhal law S_c^{α} depending on the characteristic cavity size λ, the mean flow velocity C_{ref}, the class width parameter α, and the constant $S_c \approx 86.87\ 10^{-3}$. This law applies to both the steady and the unsteady cavitation behaviors. This latter situation is, besides, characterized by the production of vapor volumes arranged into two distinct λ classes. The ratios between the mean λ values of those classes and the main cavity mean length l give values very close to $\frac{1}{3}$ and $\frac{2}{3}$, whatever the flow conditions are. The corresponding production rate is controlled by the well-known Strouhal law based on C_{ref} and l, with $S \approx 0.3$.

Combining stereometry and tomography principles, volume of transient vapor vortices is reconstructed. Despite the complexity and variety of volumes, remarkable linear relationships are found between main dimensions (chordwise, spanwise and vertical extents) and the diameter d_{eq} of a corresponding equivalent spherical volume. This applies equally to both behaviors, with specific relationships for the unsteady case.

Table 2 Mean collapse efficiency $\overline{\eta_{co}} = \overline{\hat{n}(E_d)/\hat{n}(E_c)}$

i [°]	C_{ref} [m·s^{-1}]	σ [−]	l/L [%]	$\overline{\eta_{co}}$ [−]
4°	25	1.25	20	16.5 10^{-6}
		1.12	40	69.1 10^{-6}
	32	1.26	20	122.8 10^{-6}
		1.13	40	128.6 10^{-6}

The fluid energy spectrum $\mathbf{n}(E_c)$, E_c being the potential energy of a vapor cavity, is expressed exclusively as a function of flow global parameters, production rate constant S_c, maximum potential energy E_m (defined by main cavity length l) and E_c.

The comparison between the fluid energy spectrum $\mathbf{n}(E_c)$ and the material deformation energy spectrum $\mathbf{n}(E_d)$ carried out from former pitting experiments shows a remarkable proportionality relationship defined by the collapse efficiency η_{co}. Values of η_{co} in the range 10^{-5} to 10^{-4} are found, depending on flow conditions. This relationship between the fluid and the material sides of the cavitation erosion problem confirms the well-founded nature of the energy approach and validates it.

The erosive power term P_{er} is defined as a function of flow parameters, constant S_c and of the erosive efficiency η_{er}. This efficiency is dependent upon the damaging energy threshold E_s defined by the mechanical properties of the material. A simple model based on the Rayleigh's theory is introduced that locates the erosion area according to E_s. The eroded area does not depend on the flow velocity, but essentially on the pressure gradient in the closure region of the main cavity. Quite good correlation is found with experiment.

Provided flow geometries are homologous, fluids are unchanged and cavitation coefficient is identical, the ratio between E_c spectra is equal to the ratio between velocities if velocity transposition is considered. If geometrical scale changes, the ratio between spectra per surface unit is inversely equal to the square of the geometrical ratio. Finally, the erosive power coefficient λ_{er} is introduced as to transpose P_{er}.

A study over a number of materials of engineering interest covering a wide range of mechanical properties should be engaged in order to establish correlations between these properties and E_s. Furthermore, the influence of flow parameters on the material deformation energy spectrum could be clarified in order to better understand their role on the collapse efficiency η_{co}. Finally, the determination of the maximal fluid energy E_m in relation with flow parameters is of relevance to define the upper limit of the fluid energy spectrum and thus to improve the accuracy of the erosive power term.

Acknowledgments

The authors wish to thank the members of the IMHEF cavitation research group. This work was financially supported by Électricité de France and the Swiss Federal Commission d'Encouragement à la Recherche Scientifique.

References

Avellan, F., and Farhat, M., 1989, ''Shock Pressure Generated by Cavitation Vortex Collapse,'' *International Symposium on Cavitation Noise and Erosion in Fluid Systems,* Vol. FED 88, pp. 119–125, San Francisco, ASME Winter Annual Meeting.

Baiter, H.-J., 1982, ''Estimates of the Acoustic Efficiency of Collapsing Bubbles,'' *International Symposium on Cavitation Noise,* Phoenix, AZ, ASME.

Bark, G., and Berlekom, W. B., 1978, ''Experimental Investigations of Cavitation Dynamics and Cavitation Noise,'' *12th Symposium on Naval Hydrodynamics,* pp. 470–493, Washington, D.C., ONR.

Bourdon, P., Simoneau, R., Avellan, F., and Farhat, M., 1990, ''Vibratory Characteristics of Erosive Cavitation Vortices Downstream of a Fixed Leading Edge Cavity,'' *15th Symposium on Modern Technology in Hydraulic Energy Production,* Vol. I, Belgrade (Yugoslavia), IAHR, Paper H3, 12 pp.

Brennen, C. E., 1994, ''Observations of Cavitating Flows,'' *20th Symposium on Naval Hydrodynamics,* ONR, Invited Lecture.

Ceccio, S. L., and Brennen, C. E., 1991, ''Observations of the Dynamics and Acoustics of Travelling Bubble Cavitation,'' *Journal of Fluid Mechanics,* Vol. 233, pp. 633–660.

Chahine, G. L., and Duraiswami, R., 1992, ''Dynamical Interactions in a Multi-Bubble Cloud,'' ASME JOURNAL OF FLUIDS ENGINEERING, Vol. 114, pp. 680–686.

Chien, C. H., and Aggarwal, J. K., 1985, ''Reconstruction and Matching of 3-D Objects Using Quadtrees/Octrees,'' *Third Workshop on Computer Vision,* pp. 49–54, Bellaire, MI.

Dupont, Ph., 1991, ''Étude de la Dynamique d'une Poche de Cavitation Partielle en Vue de la Prédiction de l'Érosion dans les Turbomachines Hydrauliques,'' Ph.D. thesis, École Polytechnique Fédérale de Lausanne, Institut de Machines Hydrauliques et de Mécanique des Fluides (IMHEF-LMH), No. 931.

Farge, M., 1992, ''Wavelet Transforms and their Applications to Turbulence,'' *Annual Review of Fluid Mechanics,* Vol. 24, pp. 395–457.

Farhat, M., 1994, ''Contribution à l'Étude de l'Érosion de Cavitation: Mécanismes Hydrodynamiques et Prédiction,'' Ph.D. thesis, École Polytechnique Fédérale de Lausanne, Institut de Machines Hydrauliques et de Mécanique des Fluides (IMHEF-LMH), No. 1273.

Farhat, M., Pereira, F., and Avellan, F., 1993, ''Cavitation Erosion Power as a Scaling Factor for Cavitation Erosion in Hydraulic Machines,'' *4th International Symposium on Bubble Noise and Cavitation Erosion in Fluid Systems,* Vol. FED 176, pp. 95–104, New Orleans, LA, ASME Winter Annual Meeting.

Fortes-Patella, R., 1994, ''Analyse de l'Érosion de Cavitation par Simulations Numériques d'Impacts,'' Ph.D. thesis, Institut National Polytechnique de Grenoble, CREMHyG, Grenoble, France.

Fortes-Patella, R., and Reboud, J. L., 1993, ''Numerical Analysis for Evaluating Cavitation Erosion Phenomenon,'' *Cavitation and Multiphase Flow Forum,* Washington D.C., ASME.

Franc, J. P., and Michel, J. M., 1988, ''Unsteady Attached Cavitation on an Oscillating Hydrofoil,'' *Journal of Fluid Mechanics,* Vol. 193, pp. 171–189.

Fujikawa, S., and Akamatsu, T., 1980, ''Effects of the Non-equilibrium Condensation of Vapour on the Pressure Wave Produced by the Collapse of a Bubble in a Liquid,'' *Journal of Fluid Mechanics,* Vol. 97, pp. 481–512.

Hammitt, F. G., 1963, ''Observations on Cavitation Damage in a Flowing System,'' ASME *Journal of Basic Engineering,* pp. 347–367.

Kato, H., 1975, ''A Consideration on Scaling Laws of Cavitation Erosion,'' *International Shipbuilding Progress,* Vol. 22, pp. 305–327.

Kato, H., Konno, A., Maeda, M., and Yamaguchi, H., 1996, ''Possibility of Quantitative Prediction of Cavitation Erosion Without Model Test,'' ASME JOURNAL OF FLUIDS ENGINEERING, Vol. 118, pp. 582–588.

Kiya, M., and Sasaki, K., 1983, ''Structure of a Turbulent Separation Bubble,'' *Journal of Fluid Mechanics,* Vol. 137, pp. 83–113.

Knapp, R. T., Daily, J. W., and Hammitt, F. G., 1970, ''Cavitation,'' *Engineering Societies Monographs,* McGraw-Hill, NY, 578 pp.

Kornfeld, M., and Suvorov, L., 1944, ''On the Destructive Action of Cavitation,'' *Journal of Applied Physics,* Vol. 15, pp. 495–506.

Kubota, S., Kato, H., Yamaguchi, H., and Maeda, M., 1987, ''Unsteady Structure Measurement of Cloud Cavitation on a Foil Section Using Conditional Sampling Technique,'' *International Symposium on Cavitation Research Facilities and Techniques,* Vol. FED 111, pp. 204–210, Boston, ASME.

Le, Q., Franc, J. P., and Michel, J. M., 1993, ''Partial Cavities: Global Behavior and Mean Pressure Distribution,'' ASME JOURNAL OF FLUIDS ENGINEERING, Vol. 115.

Lehman, A. F., 1966, ''Determination of Cavity Volumes Forming on a Rotating Blade,'' 11th International Towing Tank Conference, Tokyo, Japan.

Levinthal, C., and Ware, R., 1972, ''Three-dimensional Reconstruction from Serial Sections,'' *Nature,* Vol. 236, pp. 207–210.

Lewalle, J., 1994, ''Wavelet Analysis of Experimental Data: Some Methods and the Underlying Physics,'' 25th Fluid Dynamics Conference, Colorado Springs, CO, AIAA, p. 2281.

Maeda, M., Yamaguchi, H., and Kato, H., 1991, ''Laser Holography Measurement of Bubble Population in Cavitation Cloud on a Foil Section,'' *International Symposium on Cavitation,* Vol. FED 116, pp. 67–75, ASME.

Mørch, K. A., 1981, ''Cavity Cluster Dynamics and Cavitation Erosion,'' *International Cavitation and Polyphase Flow Forum,* pp. 1–10, Boulder, CO, ASME-ASCE.

N'Guyen, T. M., Franc, J.-P., and Michel, J.-M., 1987, ''On Correlating Pitting Rate and Pressure Peak Measurements in Cavitating Flows,'' *International Symposium on Cavitation Research Facilities and Techniques,* Vol. FED 57, pp. 207–216, ASME.

Pereira, F., 1997, ''Prédiction de l'Érosion de Cavitation: Approche Énergétique,'' Ph.D. thesis, École Polytechnique Fédérale de Lausanne, Institut de Machines Hydrauliques et de Mécanique des Fluides (IMHEF-LMH), No. 1592.

Rayleigh, Lord, 1917, ''On the Pressure Developed in a Liquid During the Collapse of a Spherical Void,'' *Philosophical Magazine and Journal of Science,* 34, No. 6, pp. 94–98.

Reboud, J. L., and Fortes-Patella, R., 1996, ''Étude de l'Interaction Fluide-Structure en Érosion de Cavitation,'' *Proceedings des Troisièmes Journées Cavitation,* pp. 183–192, Grenoble, SHF (Société Hydrotechnique de France).

Ross, D., 1977, ''Sound Radiation from Collapsing Cavitation Bubbles,'' 9th International Congress on Acoustics (ICA), Madrid (Spain), Paper L35, 6 pp.

Selim, S. M. A., 1985, ''A Theoretical Study on Cavitation Erosion Rate,'' Cavitation in Hydraulic Structures and Turbomachinery, Albuquerque, NM, ASCE/ASME Mechanics Conference.

Simoneau, R., Avellan, F., and Kuhn de Chizelle, Y., 1989, ''On Line Measurement of Cavitation Erosion Rate on a 2D NACA Profile,'' *International Symposium on Cavitation Noise and Erosion in Fluid Systems,* Vol. FED 88, pp. 95–102, San Francisco, ASME Winter Annual Meeting.

Soyama, H., Kato, H., and Oba, R., 1992, ''Cavitation Observations of Severely Erosive Vortex Cavitation Arising in a Centrifugal Pump,'' *3rd International Conference on Cavitation,* pp. 103–110, I.Mech.E.

Thiruvengadam, A., 1971, ''Scaling Laws for Cavitation Erosion,'' *Symposium on Flow of Water at High Speeds,* pp. 405–425, Leningrad, USSR, IUTAM.

Vogel, A., Lauterborn, W., and Timm, R., 1989, ''Optical and Acoustic Investigations of the Dynamics of Laser-Produced Cavitation Bubbles near a Solid Boundary,'' *Journal of Fluid Mechanics,* Vol. 206, pp. 299–338.